# DFT study of coadsorption of fatty acid and kerosene on fluorapatite (001) surface

## Weifan Du [1], Xianbo Li [1,3,4], Qin Zhang [2,3,4]

[1] Mining College, Guizhou University, Guiyang 550025, China

[2] Guizhou Academy of Sciences, Guiyang 550001, China

[3] National & Local Joint Laboratory of Engineering for Effective Utilization of Regional Mineral Resources from Karst Areas, Guiyang 550025, China

[4] Guizhou Key Lab of Comprehensive Utilization of Nonmetallic Mineral Resources, Guiyang 550025, China

Corresponding author: xbli3@gzu.edu.cn (Xianbo Li)

**Abstract:** The adsorption of fatty acid, kerosene and fatty acid-kerosene on fluorapatite (001) surface were investigated by density functional theory (DFT) calculations. The results showed that the single fatty acid could form stable chemisorption on fluorapatite (001) surface by the O of fatty acids bonding with Ca1 site. The single kerosene could not be stably adsorbed on fluorapatite (001) surface because the H of kerosene did not form hydrogen bond with the O of $PO_4^{3-}$ on (001) surface ($O_{surf}$). For the coadsorption conformation, the chemisorption of fatty acid-kerosene on fluorapatite (001) surface was contributed by the interaction between O of fatty acids and Ca1, the H of kerosene did not bond with the $O_{surf}$, but the carbon chain length of kerosene has a large influence on the coadsorption. Compared with the coadsorption of fatty acid-decane, the adsorption of butyric acid-tetradecane and octanoic acid-tetradecane on fluorapatite (001) surface have greater adsorption energies and overlapping region of DOS between O 2p and Ca 4d, indicating that there is a synergistic effect between fatty acid and tetradecane. Meanwhile, the collaborative effects exist between the molecules of fatty acids. The interpenetrating adsorption of fatty acid and kerosene on the fluorapatite surface could improve the adsorption strength and density. The flotation test further confirmed that the single kerosene could not collect fluorapatite, but it could be collected by the single fatty acid. Besides, the synergistic effect between fatty acid and kerosene could increase the flotation recovery of fluorapatite.

*Keywords:* fluorapatite surface, fatty acid, kerosene, coadsorption, DFT

## 1. Introduction

Phosphate ore is an important source for the production of phosphorus-containing products, which has an irreplaceable position as an industrial raw material in agriculture and chemicals (Gulluce et al., 2014; Tang et al., 2020). However, with the increasing demand for phosphate ores, the reserves of phosphate minerals are decreasing (Reis et al., 2016) and direct acidification is not suitable for low-grade ores (Ruan et al., 2019), so it is particularly important to choose reasonable methods to improve the recovery of phosphate minerals.

Froth flotation is the most effective method for beneficiation of low-grade phosphate ores (Abdel-Khalek., 2000; Cao et al., 2015; Ruan et al., 2017). This method utilizes the difference in surface wettability, surface electrical properties of phosphate mineral and gangue minerals to achieve high separation efficiency (Derhy et al., 2020). Notably, because there are some specific active groups in the collector structure (e.g., - COOH) that can chelate with the metal sites on the fluorapatite (Jiao et al., 2019), thus further changing the flotation difference between minerals. Many researchers separate phosphate minerals from gangue minerals by selecting different reagents to improve the recovery of phosphate minerals, and the main reagents include fatty acids, amines and vegetable oils (Sis et al., 2003; De Oliveira et al., 2019), they play an essential role in improving the surface hydrophobicity of phosphate minerals.

The physical and chemical properties of the mineral surface have a significant influence on the adsorption of the collector on the mineral surface, so the selection of the appropriate collector can enhance the flotation efficiency to a large extent. Fatty acids are conventional collectors used for the flotation of apatite (Li et al., 2013; Cao et al., 2016) because of their high affinity as well as a low cost (Ruan et al., 2017, Wang et al., 2019). Liu et al. (2017) reported that saponified fatty acid was used as collector, which made apatite easier to float by combining with $Ca^{2+}$ active sites on apatite surface. There are also reports about the application of mixed collectors made of fatty acids and other reagents in the field of mineral processing. Cao et al. (2016) studied the synergistic effect of fatty acids and sodium dodecyl sulfonate in the process of flotation of apatite. The addition of sodium dodecyl sulfonate can prevent excessive accumulation in the solution and improve the adsorption of fatty acids on the surface of apatite. It can be seen that fatty acid collectors still play an important role in the mineral processing of apatite.

However, fatty acids are characterized by low solubility, poor dispersibility and intolerance to low temperatures. To address these problems, kerosene is usually added as an assisted collector to change the polarity of the fatty acid molecules during flotation. Although kerosene has a low solubility as a molecular collector and is difficult to dissolve in water (Zhao et al., 2015), the oily molecules can act as a carrier in the flotation process (Zhou et al., 2017a). Ralston et al. (1984) used oil droplets for flotation of calcite, which can effectively separate quartz from calcite. Lin et al. (2018) used oil-based collectors for flotation of pyromorphite and the results showed that kerosene interacted with pyromorphite more than diesel and transformer oil.

The performance of collector is closely related to the physical and chemical properties of the mineral surface. The properties of the mineral surface are directly affected when reagent molecules are adsorbed on different terminations. Sis (2003) found that dodecane reduced the surface tension of sodium oleate solution, which has a beneficial effect on the flotation of phosphate ore. Zhou et al. (2014) found that flotation of cerium fluorocarbon ore with activated oil bubbles made of fatty acids and kerosene had a better capture capacity stronger than conventional bubbles. The addition of kerosene to the slurry increased the viscosity between the mineral surface and the flotation bubbles and enhanced the adsorption of the fatty acid collector on the mineral surface. Zhou et al. (2017a) demonstrated the strong collecting ability of these bubbles on phosphate using kerosene bubbles containing fatty acids. Sis (2001) showed that flotation of phosphate ores with non-polar oil as an auxiliary collector can reduce the amount of collector and can prevent excessive foaming. Zhu et al. (2020) mixed fatty acids with fuel oil in a certain ratio to flotation of phosphate ores and obtained 92.51% of $P_2O_5$ recovery. All the above researches show that the mixed-use of fatty acids and kerosene have a good effect on the flotation of phosphate ore, but the mechanism of the synergetic action is not clear.

Density functional theory (DFT) calculations have been applied to study the interaction between reagents (collectors, depressants, etc.) and mineral surface to reveal the essence of the reaction. Researchers have begun to transfer more interest in the field of atomistic simulation methods for surface physical-chemistry phenomena applied to froth flotation, and the number of articles containing the words "flotation" and "DFT" has shown a high growth trend in the past few years (Foucaud et al., 2019a). Especially, Foucaud et al. (2019b; 2020; 2021a) combined the spectroscopies (infrared spectroscopy, X-ray photoelectron spectroscopy) and atomistic simulations to study the synergistic adsorption of different substances on fluorite and monazite surfaces, and provided new insights for the adsorption mechanism of fatty acids and other substances on mineral surfaces. Xie et al. (2018) investigated the adsorption mechanism of fatty acids with different carbon chain lengths on the surface of fluorapatite based on DFT, and the results showed that fatty acids were chemisorbed on the mineral surface. An et al. (2021) found that the essence of synergetic mechanism of oleic acid-dodecane was that they formed a relatively ordered "supramolecular structure" on the low rank coal surface. Foucaud et al. (2021b) indicated through DFT calculation that during the hydration process of scheelite, $Ca^{2+}$ ions on the mineral surface can adsorb water molecules. Mkhonto et al. (2006) demonstrated $Ca^{2+}$ ions play a key role in the adsorption process of reagents and fluorapatite surface. These research results show that DFT calculation is a relatively mature technology for understanding the adsorption mechanisms of flotation reagents.

Nevertheless, there is rare literature about the mechanism of multiple collectors acting together on the surface of fluorapatite by DFT calculations, while conventional analytical methods such as X-ray photoelectron spectroscopy, infrared spectroscopy, and zeta potential cannot reveal the mechanism of collectors such as fatty acids and kerosene on the surface of fluorapatite from a microscopic perspective. Therefore, based on the first principles, DFT was used to calculate the adsorption energy, density of states (DOS), Mulliken bond population and bond length to reveal interatomic interactions of fatty acid and kerosene adsorption on fluorapatite surface. The research would confirm the coadsorption configuration and clarify the mechanism of adsorption and bonding between the collector and the fluorapatite surface at the molecular level.

## 2.    Materials and methods

### 2.1.  Materials

The fluorapatite mineral was collected from Guizhou Province, China. The sample was hand-picked, crushed and then ground in a ceramic ball mill. The particle size was -25 μm, and the purity of fluorapatite was 93%. Kerosene was purchased from Shanghai Macklin Biochemical Co., Ltd, China. Sodium oleate used as collector was provided by Shanghai Aladdin Biochemical Technology Co., Ltd, China. The pulp pH was adjusted by 0.1 mol/L hydrochloric acid (HCl) and 0.1 mol/L sodium hydroxide (NaOH), which were purchased from Chongqing Chuandong Chemical (Group) Co., Ltd, China. All the reagents used in this study were of analytical grade. All experiments were carried out in distilled water with an electric resistivity of 18.25 MΩ·cm.

### 2.2.  Fourier transform infrared spectroscopy analysis

The adsorption of fatty acid and kerosene on the surface of fluorapatite was analyzed by Fourier transform infrared spectroscopy (FTIR, VERTEX 70, Bruker, Germany). 0.5 g of fluorapatite samples were added to 40 mL solution which was prepared with or without fatty acid and kerosene. After magnetic stirring for 20 min, the mineral samples were filtered, and dried in a vacuum oven. Then the mineral samples were mixed with KBr and the spectra were recorded in the range of 4000–400 $cm^{-1}$ with a resolution of 4 $cm^{-1}$.

### 2.3. Micro-flotation experiments

Micro-flotation tests were conducted in a XFGCII flotation machine (Jilin Exploration Machinery Plant, China). Firstly, 2.0 g of fluorapatite samples were placed in the plexiglass cell with 40 mL distilled water. After agitation 1 min at 1992 rpm, the pH of the slurry was adjusted to about 9.5. The single kerosene, single fatty acid or mixed collector of kerosene and fatty acid at different ratio (2:8, 3:7, 4:6, 5:5, 6:4, 7:3, 8:2) was added into the cell with 2 min conditioning time, the flotation was conducted for 3 min. The froth and sink products were separately filtered, dried, weighed. The flotation recovery was calculated based on the weight of the dry products.

### 2.4. Calculation method

The simulation calculations are based on DFT (Liu et al., 2013), using the CASTEP module in Material Studio software for the geometry optimization of the cell. The exchange correlation function used is a modified approximation of the Perdew and Wang (PW91) under the generalized gradient approximation (GGA) (Wang et al., 2018), which has a high accuracy in chemisorption calculations. The energy cutoff was 380.0 eV and the K point in the Brillouin region was 2 × 2 × 2. Geometry optimization was performed using the Broyden-Fletcher-Goldfarb-Shanno (BFGS) algorithm. The maximum force was 0.5 eV/Å, the energy tolerance was $2.0×10^{-5}$ eV/atom, the maximum displacement tolerance was 0.002 Å, and the self-consistent iterative convergence accuracy was $2.0×10^{-6}$. The interaction between electron and ion nucleus is described using the ultra-soft pseudoprime (USP) (Clark et al., 2005), and it was also used for the geometry optimization, DOS and the Mulliken charges population calculations (Hossain et al., 2011). The DOS results are obtained by integrating the dispersion difference of a given frequency band in the Brillouin zone, the grid parameter was 2 × 1 × 1, the band energy tolerance was

1.0×10$^{-5}$ eV. Besides, the different chain length of fatty acids and kerosene were optimized in cubic cells of (15 × 15 × 15) Å$^3$ and (20 × 20 × 20) (Tetradecane) Å$^3$, respectively.

## 2.5. Computational models

Ideal fluorapatite cell was selected for optimization calculations and adsorption, and the cell structure was obtained from the American mineralogical crystal structure database, which was created by Comodi et al. (2001). The optimized lattice parameters of crystal structure were a=9.246 Å, b = 9.259Å, c = 6.890 Å, and α = β= 90°, γ = 120°. The size of the super cell was a=27.739 Å, b=27.777Å, c=6.890 Å. The surface structure of fluorapatite (001) is shown in Fig. 1. The (001) surface is composed of four "sublayers" and shows symmetry in space. A symmetrical surface slab model with a vacuum region of 28 Å was built, and a further geometry optimization was performed. The fluorapatite crystal structure contains two types of Ca sites (Ca1 site and Ca2 site), the Ca1 site exposed on the surface and the Ca2 site located between PO$_4^{3-}$. Previous calculations by DFT revealed that the fluorapatite (001) surface has the lowest surface energy (Clark et al., 2005). In terms of the physicochemical processes that occur when the reagent molecules are adsorbed on the mineral surface, a lower adsorption energy indicates a more stable binding between the collector and mineral surface. Therefore, the fluorapatite (001) surface was selected as the subsequent study surface. None of the Ca termination, Ca-Ca termination and O termination on the fluorapatite (001) surface expose Ca2 atoms, which allows fatty acids to interact with Ca1 atoms but not with Ca2 atoms. Xie et al. (2018) calculated the surface energies of Ca termination, Ca-Ca termination, and O termination by DFT, the values are 0.811 J/m$^2$, 1.541 J/m$^2$, and 1.425 J/m$^2$, respectively. The Ca termination has the lowest surface energy, thus the interactions between fatty acid, kerosene and the Ca termination were subsequently calculated.
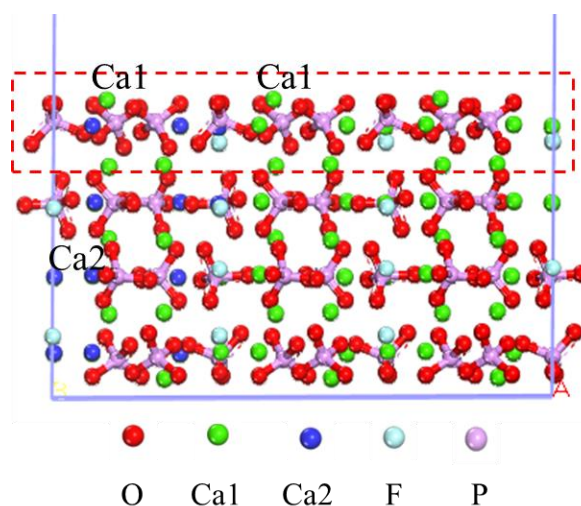


Fig. 1. Fluorapatite (001) surface structure

For the structure of fatty acid, Cooper et al. (2004) used a model of short chain fatty acid (methanoic acid) instead of oleic acid to study the interaction of the collector with the surface of fluorite (111), and found that the adsorbate containing carbonyl group interacted strongly with the surfaces. The short chain fatty acid has the same functional group (RCOO$^-$) as oleic acid, which did not affect the bonding of RCOO$^-$ on the fluorapatite surface. Besides, the chain length did not affect significantly the adsorption of a single molecule (Foucaud et al., 2018, Eskanlou et al., 2022). Therefore, in order to save calculation time and cost, the interaction between fatty acid and fluorapatite surface was studied by using short chain butyric acid and octanoic acid instead of oleic acid as collector, and the electron transfer of carboxyl group in fatty acid on the surface of fluorapatite was analysed by using Mulliken charge population. Meanwhile, decane and tetradecane with moderate carbon chain length in kerosene were selected to investigate the adsorption of fatty acids and kerosene on the fluorapatite (001) surface. Considering that fatty acids exist mainly in the form of anion (RCOO-) under alkaline conditions (Huang et al. 2021), the anionic form of butyric acid and octanoic acid were applied in the simulation calculation. Fig. 2 shows the molecular models of the free anion forms of fatty acid and kerosene.

The adsorption energy of single fatty acid or kerosene collector on the surface of fluorapatite (001), and the adsorption energy of coadsorption on (001) surface were based on equation (1) and (2), respectively (Lee et al., 2013):

$$E_{ads}=E_{collector/surf}-(E_{collector}+E_{surf}) \quad (1)$$

$$E_{ads}=E_{fatty\ acid\ +kerosene/surf}-(E_{fatty\ acid}+E_{surf}+E_{kerosene}) \quad (2)$$

where $E_{ads}$ is the adsorption energy, $E_{collector/surf}$ is the total energy of the collector after the action on the (001) surface of fluorapatite, $E_{fatty\ acid+kerosene/surf}$ is the coadsorption energy of fatty acid and kerosene on (001) surface, $E_{collector}$ is the energy of the collector (fatty acid or kerosene), $E_{fatty\ acid}$ is the energy of the fatty acid, $E_{kerosene}$ is the energy of kerosene, and $E_{surf}$ is the energy of the fluorapatite (001) surface.
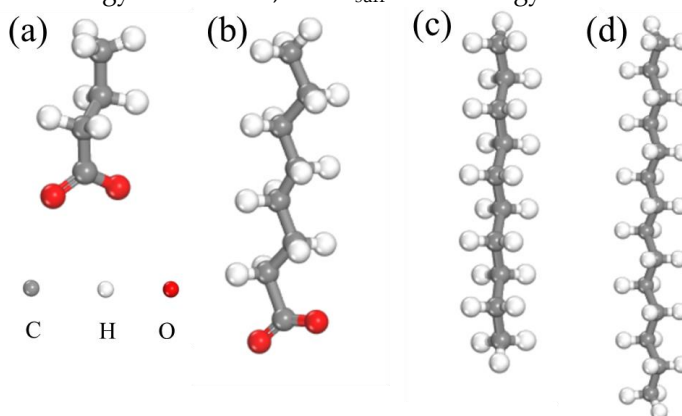


Fig. 2. Molecular models of the target collectors (a) butyric acid, (b) octanoic acid, (c) decane and (d) tetradecane

## 3.    Results and discussion

### 3.1.   Adsorption of water molecule and fatty acid on the surface of fluorapatite (001)

In alkaline solutions, the hydrogen atom of RCOOH can ionize to form RCOO⁻ (Zeng et al., 2021). O1 and O2 were defined as the O in C=O and C—O of RCOO⁻, respectively. The adsorption configurations of a single water molecule, butyric acid and octanoic acid on the Ca1 site of the fluorapatite (001) surface are presented in Fig. 3, the corresponding adsorption energies, Mulliken bond population and bond lengths are shown in Table 1. The whole adsorption system tends to form the configurations with lower energy and more stability, and the participation of fatty acids reduces the adsorption energy of the whole system, which makes the fatty acid collectors less likely to detach from the mineral surface, this means that the adsorption is more stable. The results show that butyric acid and octanoic acid could form a stable adsorption conformation on the Ca1 site. Both the O1 and O2 of fatty acids could bond with Ca1 site. When butyric acid was adsorbed on the Ca1 site, the bond length and population of O1-Ca1 and O2-Ca1 were 2.36 Å and 0.10, respectively. The values of bond population and bond lengths for octanoic acid have a little change.

Geometrically speaking, the water molecule was systematically coordinated by its oxygen atom to the surface calcium cation. Water molecule was adsorbed on Ca1 site with a distance of 2.39 Å, this value is consistent with the water molecule adsorbed on calcium cation of dolomite surface (Semmeq et al., 2021). The adsorption energy of a single water on the (001) surface is -83.80 kJ/mol, this is in good agreement with the typical values for the adsorption of the water molecules on metals/minerals surfaces, e.g. –89 kJ/mol for calcite (Rahaman et al., 2008), –80 kJ/mol for the (001) surface of scheelite (Foucaud et al., 2021b), −91.0 kJ/mol and−94.2 kJ/mol for the adsorption on magnesium and calcium cations on dolomite surface, respectively (Semmeq et al., 2021). This indicates that the fluorapatite has a strong affinity for water molecule, so the surface of natural fluorapatite is hydrophilic.

The adsorption energies of butyric acid and octanoic acid on fluorapatite (001) surface are -137.86 kJ/mol and -170.42 kJ/mol, respectively, the absolute values are higher than the adsorption energy of water molecule on the surface, which makes it possible for fatty acids draining the water molecules and adsorption on fluorapatite surface theoretically. Furthermore, it can be found that the adsorption of

butyric acid and octanoic acid on the surface of fluorapatite were mainly chemical adsorption (-80 to -400 kJ/mol) (Yu et al., 2003). It is worth noting that the absolute value of adsorption energy increases with the number of carbon atoms in the fatty acid, and the value of adsorption energy can directly reflect the stability of the adsorption conformation. The larger the difference of the total energy before and after adsorption, the more energy is released during the adsorption process. When fatty acid binds with Ca site on the surface of fluorapatite (001), alkyl groups with non-polarity are exposed to the surface, increasing the hydrophobicity of fluorapatite, which means that the long chain octanoic acid can be more firmly adsorbed on the Ca termination. However, the aliphatic chain length does not affect the adsorption mechanisms, which are mainly led by the anionic/polar carboxylic group (Foucaud et al., 2018).
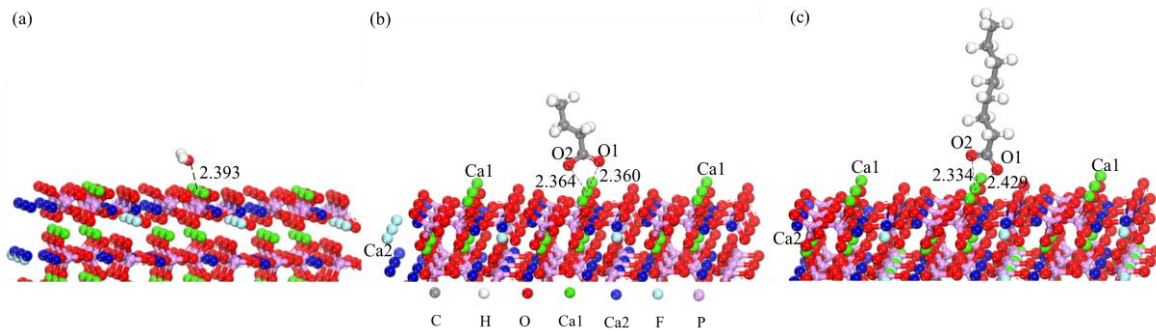


Fig. 3. Adsorption configurations of (a) single water molecule, (b) butyric acid and (c) octanoic acid on the fluorapatite (001) surface

Table 1. Adsorption energies of butyric acid and octanoic acid on fluorapatite (001) surface

| Adsorption model | Bond | Population | Length/Å | $E_{ads}$/(kJ/mol) |
|---|---|---|---|---|
| Single water molecule on (001) surface | O-Ca1 | 0.09 | 2.39 | -83.80 |
| Butyric acid on (001) surface | O1-Ca1 | 0.10 | 2.36 | -137.86 |
| | O2-Ca1 | 0.10 | 2.36 | |
| Octanoic acid on (001) surface | O1-Ca1 | 0.08 | 2.43 | -170.42 |
| | O2-Ca1 | 0.10 | 2.33 | |

Many researchers have revealed the adsorption and bonding mechanism of reagents on the mineral surface by analyzing the DOS (Nan et al., 2019; Tang et al., 2021). Fig. 4 shows the DOS for the interaction between O of fatty acid and Ca1 on fluorapatite (001) surface. The value of the Fermi energy level (Ef) was set to 0 eV. The overlapping region of O and Ca of DOS shows the orbitals where the interaction between the two atoms occurs, and the overlapping area can indicate the interaction intensity between the two atoms. The 2p orbitals of O1 and O2 are active near the Fermi energy level when fatty acids were adsorbed on the surface of fluorapatite (001), which reveals that O in fatty acids has a very active chemical energy. As indicated by the region marked in Fig. 4, there is a strong bonding between O and Ca in the range of -7.2 to 0.2 eV for butyric acid, while the octanoic acid exhibits stronger bonding in the range of -7.2 to 0.5 eV, and the antibonding interaction becomes weak in the range of 4.7 to 6.1 eV. The overlapping area between O-Ca of octanoic acid is larger and the antibonding interaction is weaker, indicating a stronger interaction between O and Ca1 site for octanoic acid. As the number of carbon atoms in the fatty acid increases, the overlapping area of the DOS between the O 2p and Ca 4d orbitals increases. Accordingly, the interaction between O and Ca is strengthened. This result is consistent with the increase of the adsorption energy of fatty acids on the surface of fluorapatite (001). Combining the adsorption effects of the two fatty acids, the adsorption conformation of octanoic acid on Ca site has lower adsorption energy and more stable adsorption.
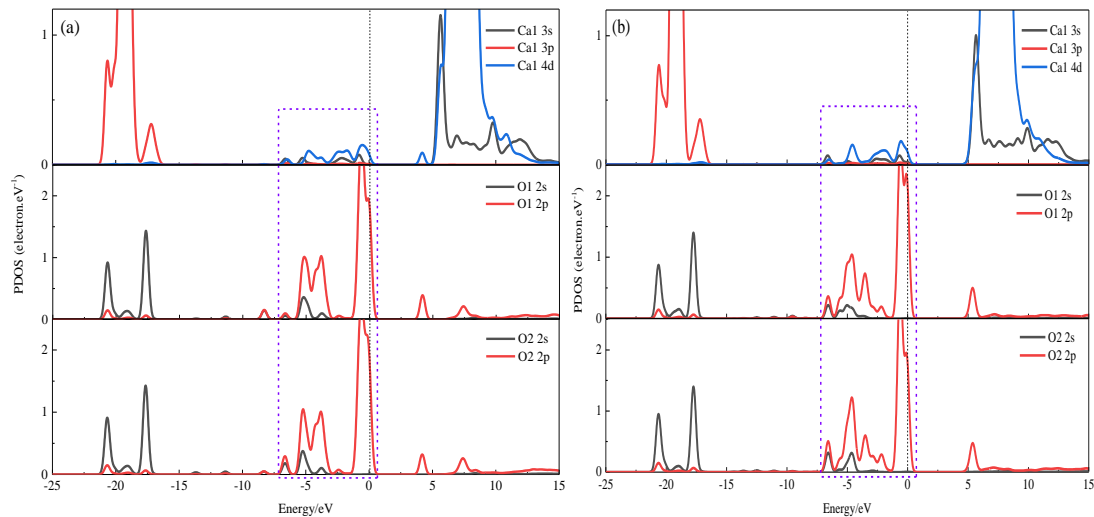
Fig. 4. PDOS of butyric acid (a) and octanoic acid (b) adsorption on fluorapatite (001) surface

### 3.2. Adsorption of kerosene on the surface of fluorapatite (001)

Kerosene is a common collector in flotation field (Al-Otoom., 2008; Li et al., 2018), which is a polyalkane mixture whose components are mainly alkanes of 8-16 carbons. Decane with 10 carbons and tetradecane with 14 carbons were used to represent the kerosene adsorption on fluorapatite (001) surface.

The adsorption configurations and adsorption energies of decane and tetradecane on the fluorapatite (001) surface are shown in Fig. 5 and Table 2, respectively. It can be seen that the distances between H of kerosene and O on fluorapatite (001) surface ($O_{surf}$) (decane:H1-O14=2.739 Å, H2-O14=2.826 Å; tetradecane:H1-O14=3.312 Å, H2-O14 =2.998 Å) are much larger than the sum of the two atomic radii, thus the H of kerosene could not form hydrogen bonds with the O in $PO_4^{3-}$ on the surface of fluorapatite (001). Furthermore, the interaction energy of decane and tetradecane on the fluorapatite (001) surface are 6.35 kJ/mol and 0.04 kJ/mol, respectively, the values are positive, indicating that kerosene has very low chemical activity and could not adsorb on fluorapatite surface. The results are consistent with industrial practice that fluorapatite cannot be recovered by flotation using kerosene alone as collector. Soto et al. (1985) found that the recovery of francolite decreased precipitously to zero when all the amine was replaced by kerosene, meanwhile kerosene was not adsorbed on francolite surface by adsorption tests. Zhou et al. (2017a) also found that the recovery of phosphate mineral is zero in the micro-flotation of phosphate mineral using oily bubbles (only kerosene), which is consistent with the law that the induction time was too long and the contact angle was zero.
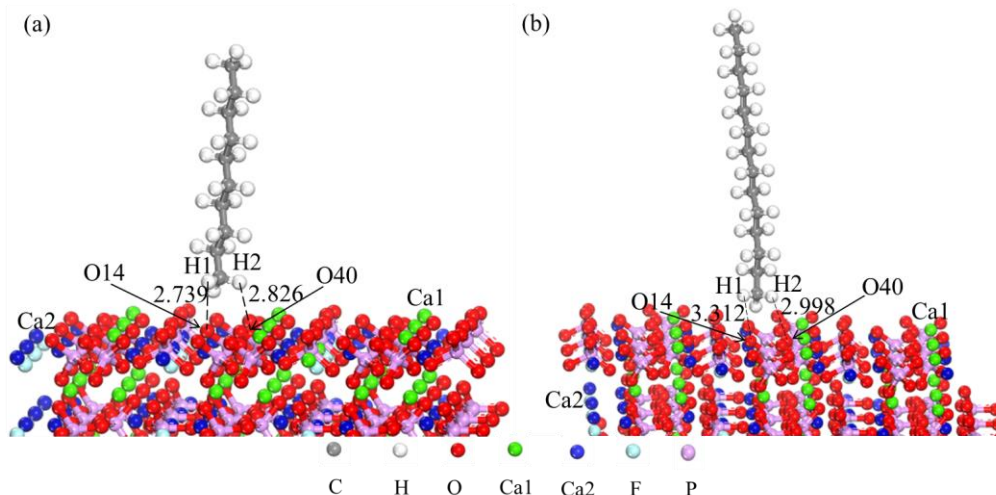


Fig. 5. Adsorption configurations of decane (a) and tetradecane (b) on fluorapatite (001) surface

Table 2. Adsorption of decane and tetradecane on fluorapatite (001) surface

| Adsorption model | Bond | Distance/Å | $E_{ads}$/(kJ/mol) |
|---|---|---|---|
| Decane on (001) surface | H1-O14 | 2.739 | 6.35 |
|  | H2-O40 | 2.826 |  |
| Tetradecane on (001) surface | H1-O14 | 3.312 | 0.04 |
|  | H2-O40 | 2.998 |  |

### 3.3. Coadsorption of fatty acids and kerosene on the fluorapatite (001) surface

Fig. 6 represents the coadsorption conformations formed by butyric acid-decane and octanoic acid-decane after optimization on the Ca termination, the coadsorption conformations of butyric acid-tetradecane and octanoic acid-tetradecane on fluorapatite (001) surface are shown in Fig. 7. The data of bond population, bond length of O-Ca$_1$ and adsorption energy are listed in Table 3, which reveals the variation of the interaction strength between the coadsorption configuration and the fluorapatite (001) surface. As can be seen from Fig.6, Fig. 7, and Table 3, for the coadsorption conformation, there is chemisorption between the fatty acid collector and fluorapatite (001) surface by the O of fatty acid bonded with the Ca$_1$, However, the H of kerosene did not bond with the O of PO$_4^{3-}$ on the Ca termination.

The energies of coadsorption of fatty acid and kerosene on fluorapatite (001) surface are shown in Table 3, the large difference in these adsorption energy values indicates that the carbon chain length of kerosene has a strong influence on fatty acids adsorption on fluorapatite (001) surface. By comparing the adsorption energies of single fatty acid in Table 1 and the fatty acid-decane on the Ca termination in Table 3, it was found that although decane did not bond with the Ca termination, it makes the absolute value of adsorption energy of the coadsorption configuration lower than that of single fatty acid on the fluorapatite (001) surface. However, for the coadsorption of fatty acid-tetradecane, the adsorption energies of butyric acid-tetradecane and octanoic acid-tetradecane on the fluorapatite (001) surface are greater than that of the single butyric acid or octanoic acid. This indicates that there is a synergistic effect between fatty acids and tetradecane, so as to obtain a more stable coadsorption configuration. Besides, compared with a single fatty acid, the coadsorption of fatty acid and kerosene will also increase the hydrophobic area of fluorapatite surface, which can strengthen the collection effect of fatty acids for fluorapatite.

On the other hand, in the case of coadsorption of the same fatty acid and kerosene, the adsorption energies of the fatty acid-tetradecane are greater than that of fatty acid-decane. Due to the similar structure of decane and tetradecane, the van der Waals force increases with the increase of the relative molecular mass of alkanes, and because both alkyl and kerosene are non-polar (Yang et al., 2013), according to the principle of similar solubility, the dispersion force between tetradecane and non-polar alkyl in octanoic acid attracts each other. This makes tetradecane and octanoic acid show stronger affinity for each other, which strengthens the adsorption energy of octanoic acid. Therefore, the increase of kerosene carbon chain length is conducive to the adsorption of fatty acids on the surface of fluorapatite. Therefore, the adsorption conformation of fatty acid-tetradecane on the Ca termination is more stable than that of fatty acid-decane conformation.

In flotation, the mineral surface is made hydrophobic by the formation of an adsorption layer, which is induced by the existence of strong lateral chain-chain interactions between molecules (Foucaud et al., 2021a). Therefore, in order to highlight the synergistic effect between the molecules of fatty acids, the adsorption of two fatty acid molecules and one kerosene molecule on the surface of fluorapatite was assessed (Fig. 8). The adsorption energy of this configuration is -220.90 kJ/mol, the absolute value is higher than the adsorption energy of a single fatty acid-kerosene molecule on the surface of fluorapatite, which demonstrates that the collaborative effects exist between the molecules of fatty acids that co-adsorb close from each other. The result is consistent with Foucaud et al. (2021a) found than stronger chain-chain interactions due to a tighter organization of the adsorbed molecules.

The fatty acid collector is bonded with the Ca site mainly by hybridization through the energy contributed between the two orbitals O 2p and Ca 4d (Xie et al., 2018). Fig. 9 is the calculated results of the DOS between O-Ca1 atoms for the coadsorption configuration of fatty acid-decane on the
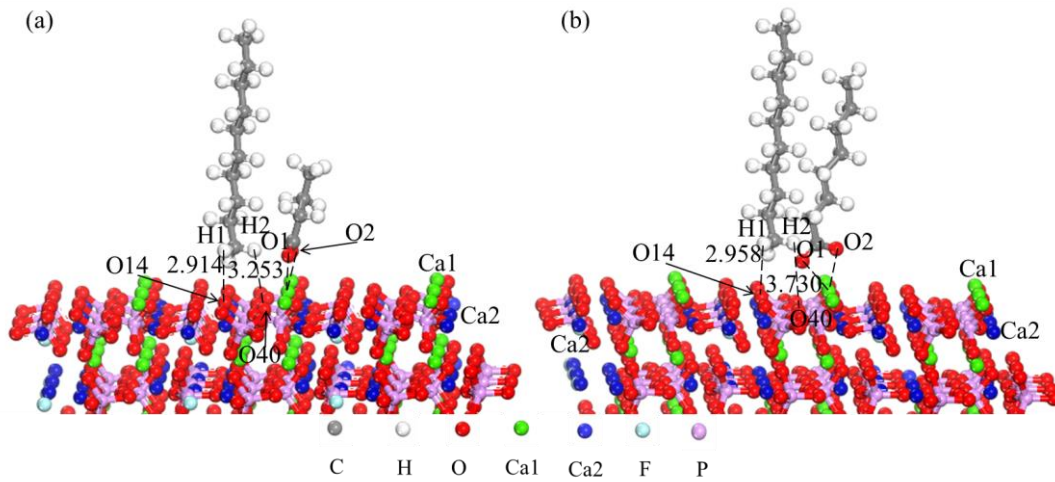
Fig. 6. Coadsorption configurations of butyric acid-decane(a), octanoic acid-decane (b) on the fluorapatite (001) surface
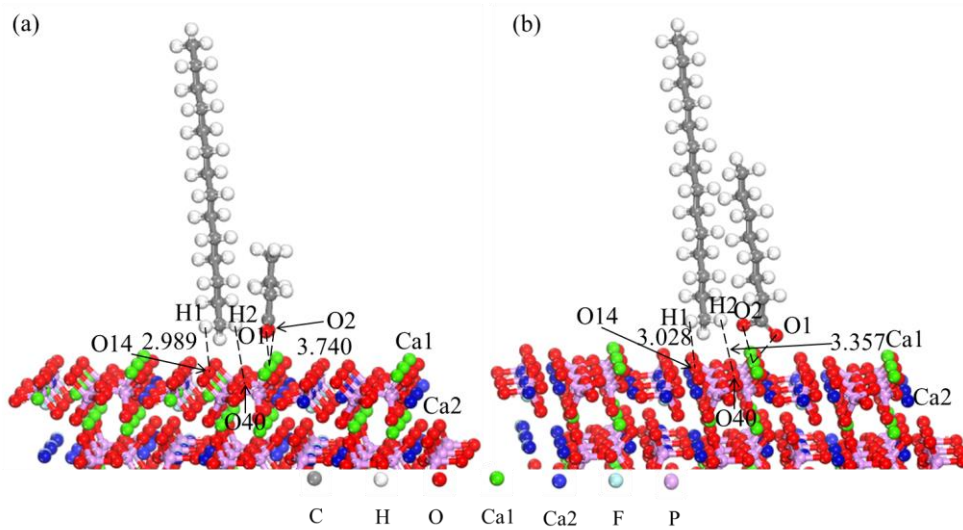


Fig. 7. Coadsorption configurations of butyric acid-tetradecane(a), octanoic acid-tetradecane (b) on fluorapatite (001) surface
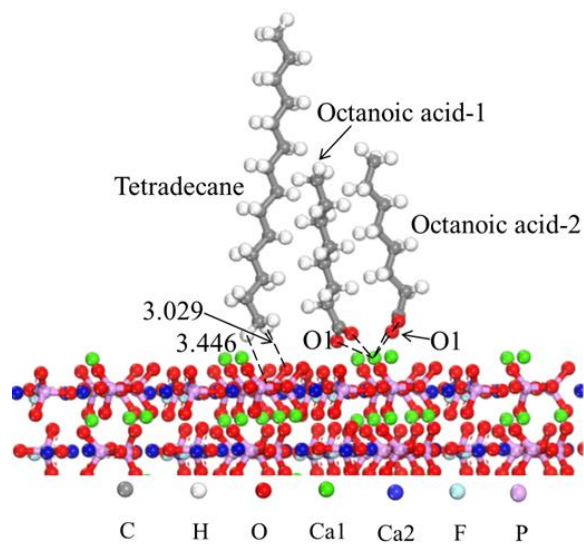


Fig. 8. Adsorption configuration of two molecular fatty acids and one molecular kerosene on (001) surface

fluorapatite (001) surface. The 2p orbitals of O1 and O2 have high energy at the Fermi energy level. The region marked in Fig. 9 shows that the O and Ca site in the butyric acid-decane coadsorption configuration have a strong bonding in the range of -6.9 to 0.2 eV. For the coadsorption conformation of octanoic acid-decane, the O and Ca exhibited a stronger bonding cooperation in the range of -7.1 to 0.4 eV. The overlapping area of O 2p and Ca 4d widened with the increase of the number of carbon atoms in the fatty acid, which indicates that the interaction between O and Ca was enhanced. The result is consistent with the adsorption energy of fatty acid interaction with the fluorapatite (001) surface.

Table 3. Coadsorption of fatty acids and kerosene on fluorapatite (001) surface

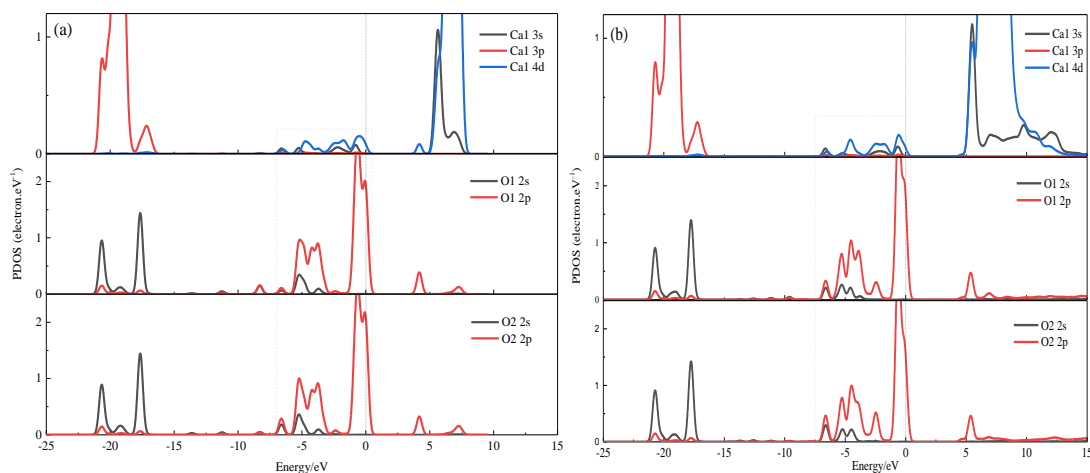| Adsorption model | Bond | Population | Length/Å | Eads/(kJ/mol) |
|---|---|---|---|---|
| Butyric acid-decane on (001) surface | O1-Ca1 | 0.10 | 2.35 | -127.34 |
| | O2-Ca1 | 0.09 | 2.42 | |
| Octanoic acid-decane on (001) surface | O1-Ca1 | 0.09 | 2.37 | -166.13 |
| | O2-Ca1 | 0.10 | 2.35 | |
| Butyric acid-tetradecane on (001) surface | O1-Ca1 | 0.10 | 2.38 | -143.92 |
| | O2-Ca1 | 0.10 | 2.38 | |
| Octanoic acid-tetradecane on (001) surface | O1-Ca1 | 0.09 | 2.39 | -181.25 |
| | O2-Ca1 | 0.10 | 2.33 | |



Fig. 9. PDOS of butyric acid-decane (a) and octanoic acid-decane (b) adsorption on fluorapatite
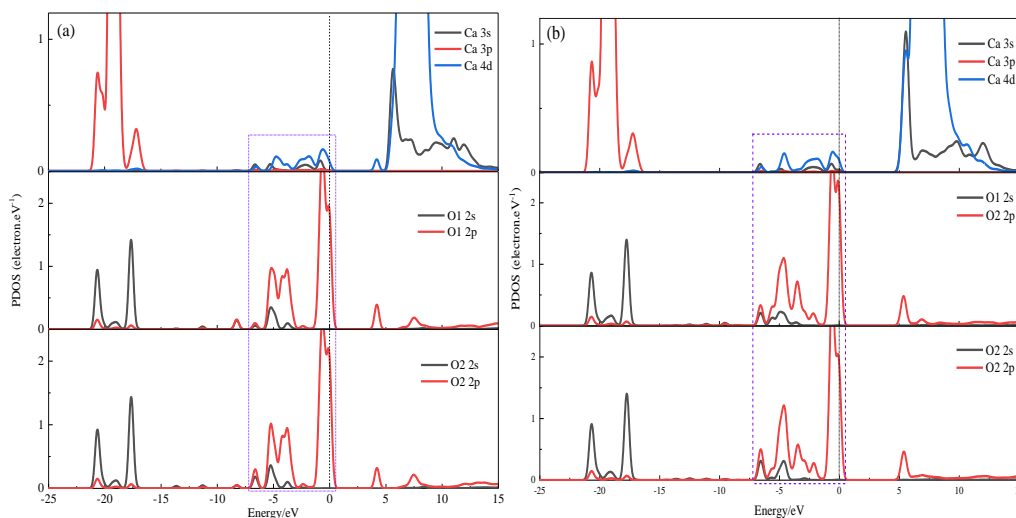


Fig. 10. PDOS of butyric acid-tetradecane (a) and octanoic acid-tetradecane (b) adsorption on fluorapatite (001) surface

Table 4 Mulliken charge population of butyric acid, octanoic acid, butyric acid-decane, octanoic acid-decane, butyric acid-tetradecane, octanoic acid-tetradecane before and after adsorption on fluorapatite (001) surface

| Adsorption model | Atom Name | Adsorption status | Valence electrons number | | | | Charge(e) |
|---|---|---|---|---|---|---|---|
| | | | s | p | d | Total | |
| Butyric acid on (001) surface | O1 | Before | 1.85 | 4.59 | 0.00 | 6.44 | -0.45 |
| | | After | 1.84 | 4.77 | 0.00 | 6.61 | -0.61 |
| | O2 | Before | 1.85 | 4.60 | 0.00 | 6.45 | -0.45 |
| | | After | 1.84 | 4.78 | 0.00 | 6.62 | -0.62 |
| | Ca | Before | 2.08 | 6.00 | 0.52 | 8.60 | 1.41 |
| | | After | 2.10 | 6.00 | 0.47 | 8.57 | 1.43 |
| Octanoic acid on (001) surface | O1 | Before | 1.84 | 4.65 | 0.00 | 6.49 | -0.49 |
| | | After | 1.83 | 4.80 | 0.00 | 6.63 | -0.63 |
| | O2 | Before | 1.84 | 4.66 | 0.00 | 6.50 | -0.50 |
| | | After | 1.83 | 4.80 | 0.00 | 6.63 | -0.64 |
| | Ca | Before | 2.08 | 6.00 | 0.52 | 8.60 | 1.41 |
| | | After | 2.10 | 6.00 | 0.48 | 8.58 | 1.42 |
| Butyric acid-decane on (001) surface | O1 | Before | 1.84 | 4.65 | 0.00 | 6.49 | -0.49 |
| | | After | 1.84 | 4.75 | 0.00 | 6.59 | -0.59 |
| | O2 | Before | 1.84 | 4.66 | 0.00 | 6.50 | -0.50 |
| | | After | 1.84 | 4.76 | 0.00 | 6.60 | -0.60 |
| | Ca | Before | 2.08 | 6.00 | 0.52 | 8.60 | 1.41 |
| | | After | 2.10 | 6.00 | 0.46 | 8.56 | 1.44 |
| Octanoic acid-decane on (001) surface | O1 | Before | 1.84 | 4.65 | 0.00 | 6.49 | -0.49 |
| | | After | 1.83 | 4.79 | 0.00 | 6.62 | -0.62 |
| | O2 | Before | 1.84 | 4.66 | 0.00 | 6.50 | -0.50 |
| | | After | 1.83 | 4.80 | 0.00 | 6.63 | -0.63 |
| | Ca | Before | 2.08 | 6.00 | 0.52 | 8.60 | 1.41 |
| | | After | 2.10 | 6.00 | 0.46 | 8.56 | 1.43 |
| Butyric acid-tetradecane on (001) surface | O1 | Before | 1.84 | 4.65 | 0.00 | 6.49 | -0.49 |
| | | After | 1.84 | 4.75 | 0.00 | 6.59 | -0.59 |
| | O2 | Before | 1.84 | 4.66 | 0.00 | 6.50 | -0.50 |
| | | After | 1.84 | 4.77 | 0.00 | 6.61 | -0.60 |
| | Ca | Before | 2.08 | 6.00 | 0.52 | 8.60 | 1.41 |
| | | After | 2.10 | 6.00 | 0.47 | 8.57 | 1.43 |
| Octanoic acid-tetradecane on (001) surface | O1 | Before | 1.84 | 4.65 | 0.00 | 6.49 | -0.49 |
| | | After | 1.83 | 4.79 | 0.00 | 6.62 | -0.62 |
| | O2 | Before | 1.84 | 4.66 | 0.00 | 6.50 | -0.50 |
| | | After | 1.83 | 4.81 | 0.00 | 6.64 | -0.64 |
| | Ca | Before | 2.08 | 6.00 | 0.52 | 8.60 | 1.41 |
| | | After | 2.10 | 6.00 | 0.47 | 8.57 | 1.43 |

The DOS of O and $Ca_1$ of butyric acid-tetradecane and octanoic acid-tetradecane are shown in Fig. 10. As can been seen from Fig. 10, the O 2p and Ca 4d exhibited a strong bonding in the range of -7.1 to 0.2 eV. Compared with the butyric acid-kerosene coadsorption conformation, the antibonding for the octanoic acid-tetradecane configuration is weaker in the range of 4.7 to 6.2 eV, and the overlapping region of DOS between O 2p and Ca 4d increases. Accordingly, the interaction between the O and $Ca_1$ was enhanced, and this result is consistent with the increase of the absolute value of adsorption energy with the increase of carbon chain length of kerosene.

Table 4 shows that the O in the butyric acid-decane adsorption on (001) surface obtained a total of 0.2 electrons, and the Ca on the fluorapatite (001) surface lost 0.03 electrons; the O in the octanoic acid-decane adsorption on (001) surface gained a total of 0.26 electrons, and the Ca lost 0.02 electrons. It demonstrates that a significant electron transfer occurs between the fatty acid collector and the Ca termination. The number of electrons transfer between octanoic acid-decane and Ca termination is higher among the two adsorption configurations, so the coadsorption configurations of octanoic acid-decane and octanoic acid-tetradecane have a lower energy.

The physicochemical heterogeneity of mineral surface is the basis for coadsorption of combined reagent. The interpenetrating adsorption configuration of fatty acid-kerosene on (001) surface of fluorapatite is presented in Fig. 11. The carboxyl group of fatty acid is a polar group, and the hydrocarbon end is a non-polar group, the unique structure makes the fatty acid show strong hydrophobicity (Zhou et al., 2014). The carboxyl group could interact with Ca site on fluorapatite surface with the non-polar group toward the outside, which makes the surface of fluorapatite tend to be non-polar and hydrophobic. Furthermore, the regions between Ca atoms were occupied by the kerosene molecule due to van der Waals force, which makes the adsorption of fatty acid more stable. Hence, the synergistic effect between fatty acid and kerosene, as well as the molecules of fatty acids could improve the adsorption strength and density of polar fatty acid on the mineral surface. The dense orientational arrangement of fatty acid and kerosene on the fluorapatite surface would enhance its hydrophobicity and form a hydrophobic film.
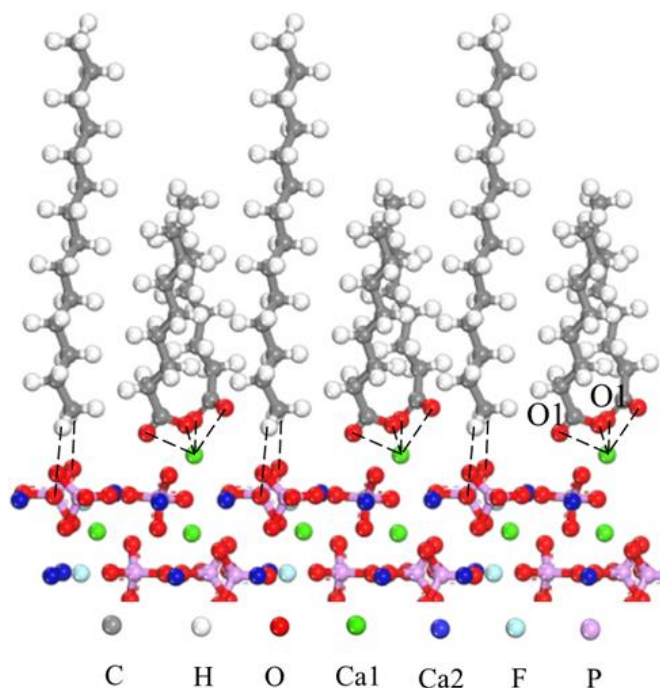


Fig. 11. Interpenetrating adsorption configuration of fatty acid-kerosene on fluorapatite (001) surface

### 3.4.  FTIR spectra analysis

The FTIR spectra was used to verify the adsorption of kerosene and fatty acid on fluorapatite surface. The FTIR spectra of fluorapatite treated with kerosene and fatty acid are shown in Fig. 12. As shown in Fig. 12a, the peaks at 572 and 604 $cm^{-1}$ are ascribed to antisymmetric bending of $PO_4^{3-}$, the peaks at 1045

and 1097 cm$^{-1}$ are corresponding to antisymmetric stretching vibration of $PO_4^{3-}$, 1429 and 1457 cm$^{-1}$ are antisymmetric stretching vibration peaks of $CO_3^{2-}$. The spectrum of fluorapatite did not change after treated with kerosene, which indicates that kerosene was not adsorbed on the surface of fluorapatite. After treated with fatty acid, the peaks at 2851, 2920 cm$^{-1}$ are ascribed to the symmetric stretching vibrations and asymmetric stretching of $-CH_2$. Besides, the asymmetric stretching of $COO^-$ appears as double peaks at 1539 and 1575 cm$^{-1}$, which was consistent with the characteristic peak of calcium dioleate (Foucaud et al., 2021a). Kou et al. (2012) also found that the reaction of sodium oleate on the hydroxyapatite surface was surface precipitation and chemisorption during the flotation of hydroxyapatite with sodium oleate. This indicates that the fatty acid was adsorbed on the surface of fluorapatite. These findings are consistent with the simulation results.
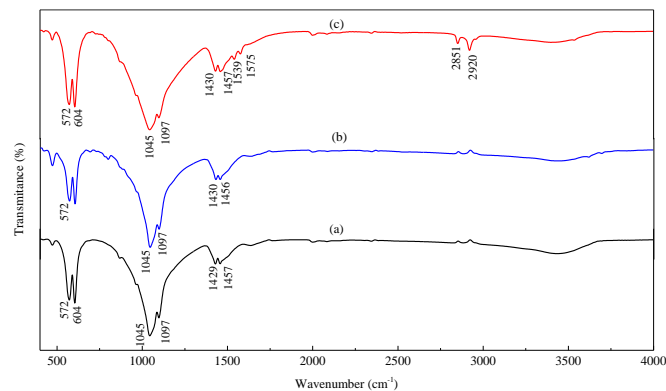


Fig. 12 FTIR spectra of (a) fluorapatite, (b) fluorapatite treated with kerosene, and (c) fluorapatite treated with fatty acid

Flotation tests of fluorapatite were carried out to confirm the synergistic effect of fatty acid and kerosene, and the results are shown in Fig. 13. As shown in Fig. 13a, when only kerosene was used as the collector, the recovery of fluorapatite was 0, which is consistent with the results reported by Zhou et al. (2017b) that the contact angle of fluorapatite surface treated with oily bubble (kerosene only) was 0°. Meanwhile, the result is consistent with the simulation result that kerosene could not be adsorbed on the surface of fluorapatite. When the fatty acid concentrations were 0.1 mg/cm$^3$ and 0.3 mg/cm$^3$, the recovery of fluorapatite were 48.63% and 75.75%, respectively. Furthermore, when the ratio of fatty acid and kerosene is 5:5, the recovery of fluorapatite were increased to 66.08% and 89.13%, respectively. This indicated that there is a synergistic effect between fatty acids and kerosene. Besides, the low ratio (less than 3:7) and high ratio (higher than 7:3) of fatty acid : kerosene was not conducive to improving the recovery of fluorapatite, the high concentration of kerosene can inhibit the formation of flotation foam. The ratio of fatty acid: kerosene between 4:6 and 6:4 could obtain high recovery.
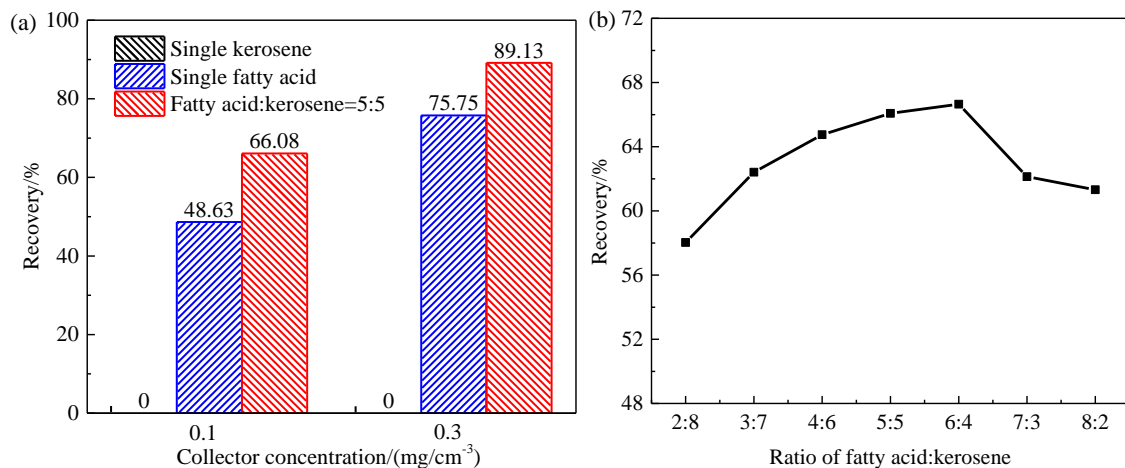


Fig. 13. Effect of the (a) collector concentration and (b) ratio of fatty acid: kerosene on flotation recovery of fluorapatite

## 4. Conclusions

The coadsorption of fatty acid-kerosene on the surface of fluorapatite (001) was investigated by DFT calculations. The adsorption energy, DOS, Mulliken electron population and Mulliken bond population were analyzed. The results showed that the single fatty acid could form a stable chemisorption on fluorapatite (001) surface by the O of fatty acids bonding with Ca1 site. The single kerosene molecule (decane, tetradecane) could not be stably adsorbed on the (001) surface of fluorapatite because the H of kerosene could not form hydrogen bonds with the O in $PO_4^{3-}$ on the surface of fluorapatite (001). FTIR spectra further demonstrates that the fatty acid was adsorbed on the surface of fluorapatite, but kerosene was not adsorbed, the recovery of fluorapatite was 0.

For the coadsorption conformation, the chemisorption of fatty acid-kerosene on fluorapatite (001) surface was caused by the interaction between O of fatty acids and Ca1, the H of kerosene did not bond with the O of $PO_4^{3-}$ on the Ca termination, but the carbon chain length of kerosene has a large influence on the coadsorption. Compared with the coadsorption of fatty acid-decane, the adsorption of butyric acid-tetradecane and octanoic acid-tetradecane on the fluorapatite (001) surface have greater adsorption energies and overlapping region of DOS between O 2p and Ca 4d, indicating that there is a synergistic effect between fatty acids and tetradecane. Meanwhile, the collaborative effects exist between the molecules of fatty acids due to chain-chain interactions. The interpenetrating adsorption with orientational arrangement of fatty acid and kerosene on the fluorapatite surface could improve the adsorption strength and density. The flotation test further confirmed that the synergistic effect between fatty acid and kerosene could increase the flotation recovery of fluorapatite. Therefore, the flotation of fluorapatite can be improved by adding the kerosene.

## Acknowledgments

## References

ABDEL-KHALEK, N.A., 2000. *Evaluation of flotation strategies for sedimentary phosphates with siliceous and carbonates gangues*. Minerals Engineering. 13, 789-793.

AL-OTOOM, A.Y., 2008. *An investigation into beneficiation of Jordanian El-Lajjun oil shale by froth floatation*. Oil Shale. 25, 247-253.

AN, M., LIAO, Y., CAO, Y., HAO, X. and MA, L., 2021. *Improving low rank coal flotation using a mixture of oleic acid and dodecane as collector: A new perspective on synergetic effect*. Processes. 9, 404-1-16.

CAO, Q., CHENG, J., WEN, S., LI, C. and LIU, J., 2016. *Synergistic effect of dodecyl sulfonate on apatite flotation with fatty acid collector*. Separation science and technology. 51, 1389-1396.

CAO, Q., CHENG, J., WEN, S., LI, C., BAI, S. and LIU, D., 2015. *A mixed collector system for phosphate flotation*. Minerals Engineering. 78, 114-121.

CLARK, S.J., SEGALL, M.D., PICKARD, C.J., HASNIP, P.J., PROBERT, M.I.J., REFSON, K. and PAYNE, M.C., 2005. *First principles methods using castep*. Zeitschrift für Kristallographie - Crystalline Materials. 220, 567-570.

COMODI, P., LIU, Y., ZANAZZI, P.F. and MONTAGNOLI, M., 2001. *Structural and vibrational behaviour of fuorapatite with pressure. Part I: in situ single-crystal X-ray diffraction investigation*. Physics and Chemistry of Minerals. 28, 219-224.

COOPER, T.G. and de LEEUW, N.H., 2004. *A computer simulation study of sorption of model flotation reagents to planar and stepped {111} surfaces of calcium fluoride*. Journal of Materials Chemistry. 14, 1927-1935.

De OLIVEIRA, P., MANSUR, H., MANSUR, A., SILVA, G.D. and PERES, A.E.C., 2019. *Apatite flotation using pataua palm tree oil as collector*. Journal of Materials Research and Technology. 8, 4612-4619.

DERHY, M., TAHA, Y., HAKKOU, R. and BENZAAZOUA, M., 2020. *Review of the main factors affecting the flotation of phosphate ores*. Minerals. 10, 1109-1-20.

ESKANLOU, A., HUANG, Q., FOUCAUD, Y., BADAWI, M. and ROMERO, A.H., 2022. *Effect of $Al^{3+}$ and $Mg^{2+}$ on the flotation of fluorapatite using fatty- and hydroxamic-acid collectors – A multiscale investigation*. Applied Surface Science. 572, 151499.

FOUCAUD, Y., BADAWI, M., FILIPPOV, L., FILIPPOVA, I. and LEBÈGUE, S., 2019a. *A review of atomistic simulation methods for surface physical-chemistry phenomena applied to froth flotation*. Minerals Engineering. 143, 106020.

FOUCAUD, Y., BADAWI, M., FILIPPOV, L.O., BARRES, O., FILIPPOVA, I.V. and LEBÈGUE, S., 2019b. *Synergistic adsorptions of Na$_2$CO$_3$ and Na$_2$SiO$_3$ on calcium minerals revealed by spectroscopic and ab initio molecular dynamics studies*. Chemical Science. 10, 9928-9940.

FOUCAUD, Y., LAINÉ, J., FILIPPOV, L.O., BARRÈS, O., KIM, W.J., FILIPPOVA, I.V., PASTORE, M., LEBÈGUE, S. and BADAWI, M., 2021a. *Adsorption mechanisms of fatty acids on fluorite unraveled by infrared spectroscopy and first-principles calculations*. Journal of Colloid and Interface Science. 583, 692-703.

FOUCAUD, Y., CANEVESI, R.L.S., CELZARD, A., FIERRO, V. and BADAWI, M., 2021b. *Hydration mechanisms of scheelite from adsorption isotherms and ab initio molecular dynamics simulations*. Applied Surface Science. 562, 150137.

FOUCAUD, Y., LEBÈGUE, S., FILIPPOV, L.O., FILIPPOVA, I.V. and BADAWI, M., 2018. *Molecular Insight into fatty acid adsorption on bare and hydrated (111) fluorite surface*. The Journal of Physical Chemistry B. 122, 12403-12410.

Geneyton, A., Foucaud, Y., Filippov, L.O., Menad, N.-E., Renard, A., Badawi, M., 2020. *Synergistic adsorption of lanthanum ions and fatty acids for efficient rare-earth phosphate recovery: Surface analysis and ab initio molecular dynamics studies.* Applied Surface Science. 526, 146725.

GULLUCE, M., BAL, T., OZKAN, H., ADIGUZEL, A., SAHIN, F. and YANMIS, D., 2014. *Conventional and molecular identification of bacteria with magnesite enrichment potential from local quarries in erzurum*. Geomicrobiology Journal. 31, 445-451.

HOSSAIN, F.M., DLUGOGORSKI, B.Z., KENNEDY, E.M., BELOVA, I.V. and MURCH, G.E., 2011. *First-principles study of the electronic, optical and bonding properties in dolomite*. Computational Materials Science. 50, 1037-1042.

HUANG, W.X., LIU, W.B., ZHONG, W.L., CHI, X.P. and RAO, F., 2021. *Effects of common ions on the flotation of fluorapatite and dolomite with oleate collector*. Minerals Engineering. 174,107213.

JIAO, F., DONG, L., QIN, W., LIU, W. and HU, C., 2019. *Flotation separation of scheelite from calcite using pectin as depressant*. Minerals Engineering. 136, 120-128.

KOU, J., TAO, D., SUN, T. and XU, G., 2012. *Application of the quartz crystal microbalance with dissipation method to a study of oleate adsorption onto a hydroxyapatite surface*. Minerals & Metallurgical Processing. 29, 47-55.

LEE, S.G., CHOI, J.I., KOH, W. and JANG, S.S., 2013. *Adsorption of β-d-glucose and cellobiose on kaolinite surfaces: Density functional theory (DFT) approach*. Applied Clay Science. 71, 73-81.

LI, C.X., CHENG, R.J. and LUO, H.H., 2013. *Study on collector for reverse flotation of certain phosphorite in Guizhou*. Advanced Materials Research. 734-737, 1086-1092.

LI, H., LIU, M. and LIU, Q., 2018. *The effect of non-polar oil on fine hematite flocculation and flotation using sodium oleate or hydroxamic acids as a collector*. Minerals Engineering. 119, 105-115.

LIN, Q., GU, G., WANG, H., LIU, Y., FU, J. and WANG, C., 2018. *Flotation mechanisms of molybdenite fines by neutral oils*. International Journal of Minerals, Metallurgy, and Materials. 25, 1-10.

LIU, W., XU, S., ZHAO, X., YUAN, G. and MIMURA, H., 2013. *Adsorption mechanism of chlorides on carbon nanotubes based on first-principles calculations*. Chemical Physics Letters. 580, 94-98.

LIU, X., LI, C., LUO, H., CHENG, R. and LIU, F., 2017. *Selective reverse flotation of apatite from dolomite in collophanite ore using saponified gutter oil fatty acid as a collector*. International Journal of Mineral Processing. 165, 20-27.

MKHONTO, D., NGOEPE, P.E., COOPER, T.G. and de LEEUW, N.H., 2006. *A computer modelling study of the interaction of organic adsorbates with fluorapatite surfaces*. Physics and Chemistry of Minerals. 33, 314-331.

NAN, N., ZHU, Y., HAN, Y. and LIU, J., 2019. *Molecular modeling of interactions between N-(carboxymethyl)-N-tetradecylglycine and fluorapatite*. Minerals. 9, 278.

RAHAMAN, A., GRASSIAN, V.H., MARGULIS, C.J., 2008. Dynamics of water adsorption onto a calcite surface as a function of relative humidity, Journal of Physical Chemistry C. 112, 2109–2115.

RALSTON, J., KENT, W. and NEWCOMBE, G., 1984. *Polymer-stabilized emulsions and fine-particle recovery,I. The calcite-quartz system*. International Journal of Mineral Processing. 13, 167-186.

REIS, A.S. and BARROZO, M.A.S., 2016. *A study on bubble formation and its relation with the performance of apatite flotation*. Separation and Purification Technology. 161, 112-120.

RUAN, Y., HE, D. and CHI, R., 2019. *Review on beneficiation techniques and reagents used for phosphate ores*. Minerals. 9, 253-1-18.

RUAN, Y., ZHANG, Z., LUO, H., XIAO, C., ZHOU, F. and CHI, R., 2017. *Ambient temperature flotation of sedimentary phosphate ore using cottonseed oil as a collector*. Minerals. 7, 65-1-14.

SEMMEQ, A., FOUCAUD, Y., EL YAMAMI, N., MICHAILOVSKI, A., LEBÈGUE, S. and BADAWI, M., 2021. *Hydration of magnesite and dolomite minerals: new insights from ab initio molecular dynamics*. Colloids and Surfaces

A: Physicochemical and Engineering Aspects. 631, 127697.

SIS, H., 2001. Enhance flotation recovery of phosphate ores using nonionic surfactants, The Pennsylvania State University.

SIS, H. and CHANDER, S., 2003. *Improving froth characteristics and flotation recovery of phosphate ores with nonionic surfactants*. Minerals Engineering. 16, 587-595.

SOTO, H. and IWASAKI, I., 1985. *Flotation of apatite from calcareous ores with primary amines*. Mining, Metallurgy & Exploration. 2, 160-166.

TANG, Y., SUN, H., YIN, W., YANG, B., CAO, S., WANG, D. and KELEBEK, S., 2021. *Computational modeling of cetyl phosphate adsorption on magnesite (104) surface*. Minerals Engineering. 171, 107123.

TANG, Y., YIN, W. and KELEBEK, S., 2020. *Selective flotation of magnesite from calcite using potassium cetyl phosphate as a collector in the presence of sodium silicate*. Minerals Engineering. 146, 106154.

WANG, L., TIAN, M., KHOSO, S.A., HU, Y., SUN, W. and GAO, Z., 2019. *Improved flotation separation of apatite from calcite with benzohydroxamic acid collector*. Mineral Processing and Extractive Metallurgy Review. 40, 427-436.

WANG, X., ZHANG, Q., LI, X., YE, J. and LI, L., 2018. *Structural and electronic properties of different terminations for quartz (001) surfaces as well as water molecule adsorption on It: A first-principles study*. Minerals. 8, 58-1-16.

XIE, J., LI, X., MAO, S., LI, L., KE, B. and ZHANG, Q., 2018. *Effects of structure of fatty acid collectors on the adsorption of fluorapatite (0 0 1) surface: A first-principles calculations*. Applied Surface Science. 444, 699-709.

YANG, J.L., DU, M.L., LIU, J. and YU, C.X., 2013. *Study on drainage oil to prepare collectors of coal flotation*. Advanced Materials Research. 734-737, 901-905.

YU, Y., ZHANG, Y., WANG, Z. and QIU, M., 2003. *Adsorption of water-soluble dyes onto modified resin*. Chemosphere. 54, 425-430.

ZENG, M., YANG, B., GUAN, Z., ZENG, L., LUO, H. and DENG, B., 2021. *The selective adsorption of xanthan gum on dolomite and its implication in the flotation separation of dolomite from apatite*. Applied Surface Science. 551, 149301-1-10.

ZHAO, W., WANG, Z., WANG, D., LI, J., LI, Y. and HU, G., 2015. *Contribution and significance of dispersed liquid hydrocarbons to reservoir formation*. Petroleum Exploration and Development. 42, 439-453.

ZHOU, F., WANG, L., XU, Z., LIU, Q. and CHI, R., 2015. *Reactive oily bubble technology for flotation of apatite, dolomite and quartz*. International Journal of Mineral Processing.

ZHOU, F., WANG, L., XU, Z., LIU, Q., DENG, M. and CHI, R., 2014. *Application of reactive oily bubbles to bastnaesite flotation*. Minerals Engineering. 64, 139-145.

ZHOU, F., WANG, L., XU, Z., RUAN, Y. and CHI, R., 2017a. *A study on novel reactive oily bubble technology enhanced collophane flotation*. International Journal of Mineral Processing. 169, 85-90.

ZHOU, F., WANG, L., XU, Z., RUAN, Y., ZHANG, Z. and CHI, R., 2017b. *Role of reactive oily bubble in apatite flotation*. Colloids and Surfaces A: Physicochem. Eng. Aspects. 513, 11-19.

ZHU, Z., ZHANG, J., ZHOU, R., DENG, X. and GUO, W., 2020. *Experimental study on application of new fatty acid collectors in flotation of a low grade collophanite ore*. Industrial Minerals & Processing. 49, 22-24.